Metals & corrosion

On the grain boundary network characteristics in a dual phase steel

Prashant Pathak[1,2], Ilana Timokhina[1], Subrata Mukherjee[2], Gregory S. Rohrer[3], and Hossein Beladi[1,*] (iD)

[1] *Institute for Frontier Materials, Deakin University, Geelong, VIC 3216, Australia*
[2] *Research and Development Division, Tata Steel Ltd., Jamshedpur 831007, India*
[3] *Department of Materials Science and Engineering, Carnegie Mellon University, Pittsburgh, PA 15213-3890, USA*
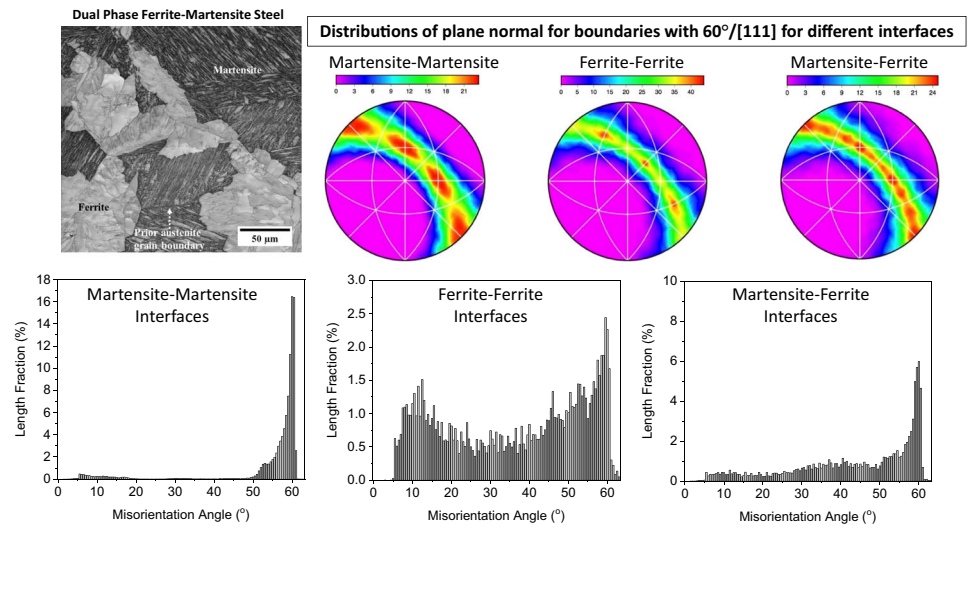
ABSTRACT

The relative areas of interfaces in dual-phase steel containing an equal fraction of ferrite and martensite have been measured and classified according to five crystallographic interface parameters. When the martensite–martensite (M–M), ferrite–ferrite (F–F), and ferrite–martensite (F–M) interfaces were analysed separately, it was apparent that the distribution in each category was determined by the dominant phase transformation mechanism (diffusional vs displacive) upon the formation of a given phase (ferrite vs martensite). The misorientation angle distribution of the M–M interfaces showed a bimodal distribution, with one mode in the range of 5°–22° and the second mode in the range of 45° to 60°, with a significant peak at ∼ 60°. The F–F interfaces were spread across all misorientation angles, revealing two broad peaks at ∼ 13° and ∼ 60°. The F–M interfaces displayed a mixed character inherited from both martensite and ferrite interfaces. The grain boundary plane distribution was also anisotropic. For example, the relative area of M–M interfaces terminated on {110} planes was greater than two multiples of a random distribution (MRD). The 60°/[111] misorientation revealed symmetrical tilt {112} boundary planes for the F–F interfaces with a relative area > 40 MRD, which correspond well with the low energy configuration, whereas the most common M–M interfaces were symmetrical tilt {110} boundaries with a relative area > 20 MRD, that result from the crystallographic constraint associated with the displacive transformation. For the case of F–M interfaces, the 60°/[111] misorientation exhibited multiple peaks spread along the zone of tilt boundaries, inherited from both diffusional ferrite and displacive martensite phase transformations.

Handling Editor: Avinash Dongare.

Address correspondence to E-mail: hossein.beladi@deakin.edu.au

GRAPHICAL ABSTRACT

Dual Phase Ferrite-Martensite Steel

Distributions of plane normal for boundaries with 60°/[111] for different interfaces

Martensite-Martensite   Ferrite-Ferrite   Martensite-Ferrite

Martensite-Martensite Interfaces

Ferrite-Ferrite Interfaces

Martensite-Ferrite Interfaces

Introduction

The use of advanced high-strength steel with an excellent combination of high strength and ductility is increasing in the automotive industry due to the demand for lighter vehicles to reduce CO_2 emissions, increase fuel efficiency, and improve crashworthiness to ensure passenger safety [1]. Dual-phase (DP) steels belong to the class of such advanced high strength steels that consist of an inherently soft ferrite phase as a matrix and hard martensite as a second phase. The combination of these microstructure constituents leads to a unique combination of properties including high strength, low yield-to-ultimate strength, continuous yielding, and high initial work hardening rate, which make DP steels popular in a wide range of structural components in an automobile [2–4]. Although DP steels exhibit a good combination of the aforementioned properties, their application is limited for the complex components requiring high formability (because of limited flangeability due to coexistence of soft and hard phases in the microstructure).

Extensive research has been carried out to understand damage initiation and fracture in DP steels upon plastic deformation (i.e., forming) [1, 5, 6]. The nucleation of voids largely occurs at ferrite–martensite (F–M) interfaces in DP steels due to the build-up of hydrostatic pressure (i.e., strain partitioning) between the hard (martensite) and soft (ferrite) phases [4]. However, the microstructure characteristics in DP steel (i.e., martensite phase distribution) appear to strongly influence the propensity of interface/interphase boundary to the void formation. In the case of isolated martensite islands surrounded by the ferrite phase, the formation of microvoids is observed at both F–M interfaces [3, 6–8] and ferrite–ferrite (F–F) boundaries [4]. However, the presence of martensite in a chain-like network in the microstructure leads to the preferential nucleation of micro-voids at the hard martensite islands (i.e., martensite–martensite (M–M) interfaces) [7]. This may be due to the change in the strain partitioning pattern as a result of the alteration in the martensite island distribution. It should be also emphasised that voids do not form at all interface/interphase boundaries during plastic deformation even up to fracture, suggesting that the strain partitioning is to some extent affected by the interface boundary character. This is consistent with a simulation conducted on a single-phase microstructure with different grain boundary networks (population and plane orientation) having a fixed texture and grain size, where the extent of elastic energy within

the microstructure strongly depends on the boundary type [9]. This strengthens the viewpoint that the grain boundary characteristics influence the overall material properties. Therefore, it is important to investigate the characteristics of interfaces in DP steel, where each microstructure constituent is formed through different phase transformation mechanisms (i.e., shear versus diffusion).

Recent technological advancements in orientation imaging analysis, with the integration of conventional electron back-scatter diffraction (EBSD) mapping and automated stereological analysis, have made it possible to measure the five crystallographic parameters required to define the grain boundary characteristics [10]. This was earlier accomplished with the more complex and time-intensive three-dimensional EBSD [11, 12] or transmission electron microscopy techniques [13]. The five-parameter approach was previously used for the grain boundary characterization of different materials including steel [10, 11, 14–16], where the first three parameters define the misorientation angle/axis (i.e., lattice misorientation or three Euler angles), while the latter two specifies the orientation of the grain boundary plane. The objective of the present work was to study the grain boundary character distribution for the three different types of interfaces namely F–F, F–M and M–M developed as a result of two distinct phase transformation mechanisms taking place during the formation of duplex microstructure in DP steels.

Experimental procedure

The steel composition used in the present study was 0.08% C, 1.58% Mn, 0.3% Si, 0.17% Ti, 0.20% Mo (wt.%), which is prone to interphase precipitation during the ferrite transformation [17]. The steel was made in a vacuum induction melting furnace, producing an approximately 100 kg ingot. It was then reheated to a temperature of 1250 °C and held for 120 min in a muffle furnace, followed by successive hot rolling reductions at a temperature range of 1100–980 °C to obtain a plate with a thickness of 30 mm. The samples were machined from the hot-rolled plate with a length of 20 mm, width of 15 mm and height of 15 mm along the rolling direction (RD), transverse direction (TD) and normal direction (ND), respectively. The thermomechanical simulation was

carried out using the hydra wedge unit of the Gleeble 3800.

Two samples were reheated to 1250 °C at a rate of 10 °C/s and held for 180 s. One sample was quenched immediately from 1250 °C to room temperature to obtain a fully martensitic microstructure to measure the prior austenite grain size. The other sample was cooled at a rate of 10 °C/s to an isothermal temperature of 625 °C and held for 810 s. Then, the sample was immediately water-quenched to room temperature to produce a dual-phase microstructure containing ferrite and martensite with approximately equal fractions (Fig. 1). The temperature of the specimen was recorded during the experiment by an R-type thermocouple welded at the centre of the test specimen.

A thin slice was cut from the heat-treated samples and mounted with the RD-ND plane parallel to the mount surface. They were initially ground using 600 and 1200 grit sandpapers, followed by polishing with the use of polishing suspensions of 9, 3, 1 μm in successive steps. The EBSD sample was further polished using OPS solution followed by ultrasonic cleaning.

The fully martensitic sample was etched by a solution, comprising 4 g of sodium dodecylbenzene in 100 ml of saturated aqueous picric acid diluted in 100 ml of distilled water with few drops of a
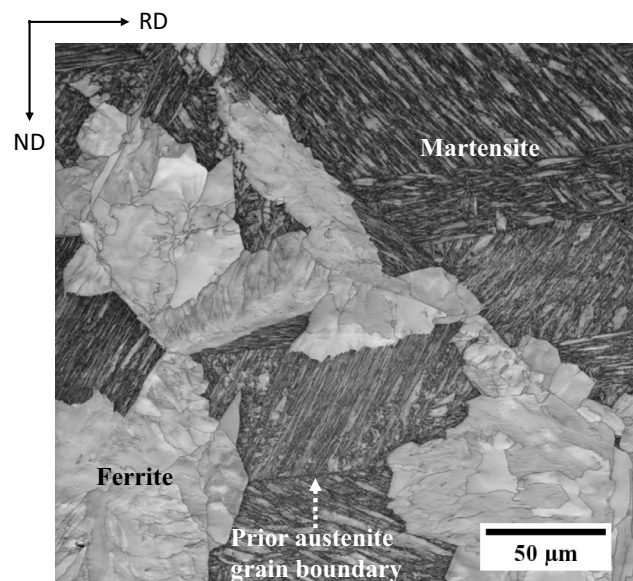
Figure 1 The image quality map of ferrite–martensite dual phase microstructure. RD and ND represent rolling direction and normal direction, respectively.

surfactant (Triton X-100), at 60 °C for ∼ 60 s to reveal the prior austenite grain boundaries. The prior austenite grain size was measured using the linear intercept method.

The EBSD measurements were carried out using an FEI Quanta 3D SEM with an operating voltage of 20 kV and a beam current of 4 nA. The EBSD maps were acquired by running the multiple scans covering the total area of ∼ 3.7 mm² (i.e., $130 \times 240 \times 120$ μm²) using a step size of 0.15 μm on a hexagonal grid. The average confidence index was in the range of 0.5–0.85. The post-processing of the data was carried out using the TSL software. The raw scanned data were subjected to multiple cleaning steps before extracting the boundary segments, using the clean-up function of the software. In the first step, a single iteration dilation clean-up routine was employed using a grain tolerance angle of 5° and minimum grain size of 5 pixels to minimise noise or ambiguous data from the orientation map. This process changes less than 2% of data points on average, depending on the EBSD map confidence index. It was followed by the single orientation function, assigning a single orientation to an individual grain by averaging all orientation data associated with it. Subsequently, the reconstructed grain boundary function with a boundary deviation limit of 2 times the step size ($2 \times 0.15 = 0.30$ μm) was used to smooth uneven grain boundaries and extract all of the grain boundary line segments (∼ 829000) from 123 EBSD images similar to the one illustrated in Fig. 1.

The dual-phase (i.e., martensite and ferrite) microstructure led to the presence of three different interfaces, consisting of F–F, F–M and M–M. Therefore, the crop function was used to separate each phase in the microstructure (i.e., ferrite grains and martensite islands). Then, the aforementioned procedures were repeated to extract the boundary segments for each microstructure constituent (i.e., M–M and F–F interfaces). The number of boundary segments for M–M and F–F interfaces was ∼ 758000 and ∼ 53000, respectively. Afterwards, in-house software was used to extract the F–M interfaces by subtracting the M–M and F–F interfaces from all boundary interfaces data. In total, there were ∼ 60000 F–M interfaces. The five-parameter grain boundary character distribution was determined from each set of grain boundary line segments using the stereological method [18]. In the current study, the five-parameter distribution was calculated using

11 bins per 90° (∼ 8.2° resolution) for the set of all boundaries and for the M–M interfaces. However, the distribution was calculated using 9 bins per 90° (∼ 10° resolution) for the F–F and F–M interfaces.

Results

The heat treatment schedule resulted in a dual-phase microstructure consisting of polygonal ferrite and lath martensite in approximately equal proportions (Fig. 1). The ferrite appeared to originate at the prior austenite grain boundaries and propagate towards austenite grain interiors. However, the prior austenite grain boundary was occasionally observed free of ferrite (as shown by an arrow in Fig. 1). The mean ferrite grain size was 19.5 ± 1.75 μm.

Misorientation angle distribution

The overall misorientation angle distribution for the dual-phase microstructure revealed a significant peak at misorientations of 55 to 60°. The distribution of boundaries from 0 to 50° was nearly flat and less than 1% in population (Fig. 2a). The misorientation angle distribution of M–M boundaries was similar to that of the overall microstructure (Fig. 2b). However, very few boundaries are found between 20° and 50° and the maxima at ∼ 60° was about ∼ 16%, compared to ∼ 14% in the overall microstructure.

The misorientation angle distribution of F–F boundaries was found to be significantly different from the ones discussed above. The population of these interfaces was found to be mostly in two broad peaks centred at disorientation angles of ∼ 13° and 60°, with maxima of approximately 1.5% and 3% of the total population, respectively. Note that the peak at 60° is significantly less than the one observed for the overall and M–M interfaces (Fig. 2). Also, there was a considerable rise in the boundary population lying in the misorientation angle range of 20–50°. The F–M misorientation angle distribution also had a maximum at 60°, although it is not as large as for the overall and M–M distributions. The population corresponding to these interfaces constituted about 6% of the total F–M interface. The population of the interfaces corresponding to the misorientation angle between 0–50° is less than 2% (Fig. 2d).
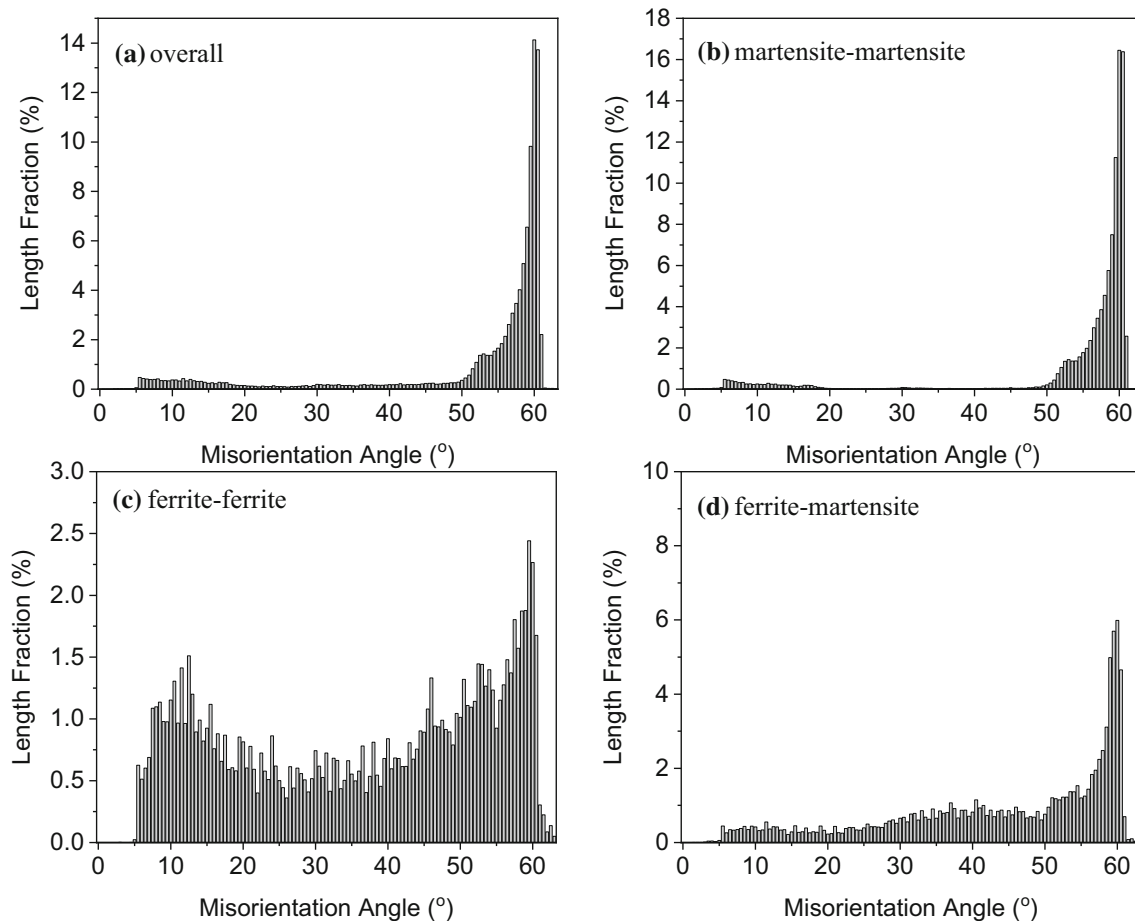
Figure 2 Misorientation angle distribution for different interfaces in the dual phase steel.

The intervariant interface length distribution

The transformed phases (martensite and ferrite) share a specific orientation relationship (OR) with the parent phase, which can be the Kurdjumov–Sachs (K–S), Nishiyama–Wasserman (N–W), Pitch (P) and Greninger–Troiano (G–T) orientation relationships [10]. Previous work on the low carbon steels has demonstrated that the orientation relationship of the transformed phase and parent austenite is very close to the K–S OR [10, 19]. There are 24 unique crystallographically possible ferrite/martensite variants of the K–S OR (as detailed in Table 1), which can be formed from a specific austenite grain/orientation based on the crystal symmetry of the cubic system. These 24 variants can further be divided into four groups also known as "packets" consisting of six variants (e.g., V1–V6), with their common plane parallel to the closed packed planes of the parent phase. The intersection/interaction between these variants results in

23 misorientation axis-angle combinations when V1 is used as a reference. However, because of the symmetry of the cubic system, some of these intervariant interfaces (e.g., V1–V3 and V1–V5 = 60°/[011]) are identical [10, 20] and hence, there are only 16 distinct misorientation angle-axis combinations.

The results from the analysis of three different types of interfaces (i.e., martensite–martensite, ferrite–ferrite and ferrite–martensite) along with overall microstructure and theoretical are presented in Fig. 3. The theoretical calculation assumes that each variant has equal chance to form within a parent austenite grain upon the phase transformation. The overall microstructure involving all the interfaces was dominated by the presence of V1–V3 (i.e., 60°/[011]) intervariant interfaces, which constitutes 42% of the total population (Fig. 3). The M–M interfaces showed the presence of all the six variants that belong to the same closed packed group i.e., V1 through V6. However, the intervariant interfaces represented by

Table 1 Possible 24 variants generated through fcc-to-bcc phase transformation having the KS orientation relationship

Variant	CSL	Bain group	Plane Parallel	Direction Parallel	Rotation angle /Axis from V1
V1		B1	$(111)_\gamma\|\|(011)_\alpha$	$[-101]_\gamma\|\|[-1-11]_\alpha$	–
V2	$\Sigma3$	B2		$[-101]_\gamma\|\|[-11-1]_\alpha$	60°/[11−1]
V3		B3		$[01-1]_\gamma\|\|[-1-11]_\alpha$	60°/[011]
V4	$\Sigma1$	B1		$[01-1]_\gamma\|\|[-11-1]_\alpha$	10.5°/[0−1−1]
V5		B2		$[1-10]_\gamma\|\|[-1-11]_\alpha$	60°/[0−1−1]
V6	$\Sigma11$	B3		$[1-10]_\gamma\|\|[-11-1]_\alpha$	49.5°/[011]
V7	$\Sigma19b$	B2	$(1-11)_\gamma\|\|(011)_\alpha$	$[10-1]_\gamma\|\|[-1-11]_\alpha$	49.5°/[−1−11]
V8	$\Sigma1$	B1		$[10-1]_\gamma\|\|[-11-1]_\alpha$	10.5°/[11−1]
V9		B3		$[-1-10]_\gamma\|\|[-1-11]_\alpha$	50.5°/[−10 3 −13]
V10		B2		$[-1-10]_\gamma\|\|[-11-1]_\alpha$	50.5°/[−7 −5 5]
V11	$\Sigma1$	B1		$[011]_\gamma\|\|[-1-11]_\alpha$	14.9°/[13 5 1]
V12		B3		$[011]_\gamma\|\|[-11-1]_\alpha$	57.2°/[−356]
V13	$\Sigma1$	B1	$(-111)_\gamma\|\|(011)_\alpha$	$[0-11]_\gamma\|\|[-1-11]_\alpha$	14.9°/[5 −13 −1]
V14		B3		$[0-11]_\gamma\|\|[-11-1]_\alpha$	50.5°/[−55 −7]
V15		B2		$[-10-1]_\gamma\|\|[-1-11]_\alpha$	57.2°/[−6−25]
V16		B1		$[-10-1]_\gamma\|\|[-11-1]_\alpha$	20.6°/[11 −11 −6]
V17		B3		$[110]_\gamma\|\|[-1-11]_\alpha$	51.7°/[−11 6 −11]
V18		B2		$[110]_\gamma\|\|[-11-1]_\alpha$	47.1°/[−24 −10 21]
V19		B3	$(11-1)_\gamma\|\|(011)_\alpha$	$[-110]_\gamma\|\|[-1-11]_\alpha$	50.5°/[−3 13 10]
V20		B2		$[-110]_\gamma\|\|[-11-1]_\alpha$	57.2°/[3 6 −5]
V21		B1		$[0-1-1]_\gamma\|\|[-1-11]_\alpha$	20.6°/[30−1]
V22		B3		$[0-1-1]_\gamma\|\|[-11-1]_\alpha$	47.1°/[−10 21 24]
V23		B2		$[101]_\gamma\|\|[-1-11]_\alpha$	57.2°/[−2 −5 −6]
V24		B1		$[101]_\gamma\|\|[-11-1]_\alpha$	21.1°/[9 −4 0]

V1-V3 (i.e. 60°/[011]) constituted the majority, accounting for more than 50% of the total population, followed by the population of twin-related inter-variant boundaries V1-V2 (i.e., 60°/[11−1]). The other intervariant interfaces had a fraction of less than 3%.

In case of F–F interfaces, the population was predominantly distributed between V1- V4 (i.e. 10.53°/ [0−1−1]), V1-V8 (i.e., 10.53°/[11−1]) and V1–V11 (i.e., 14.9°/[13 5 1]) intervariant interfaces with the values of about 13, 10 and 9%, respectively (Fig. 3). The pairing of intervariants for F–M interfaces showed a trend similar to the M–M interfaces with the highest fraction observed for 60°/[011] (about 13%), followed by intervariant interfaces V1-V15 (i.e., 57.21°/ [−6−25]) and V1-V2 (i.e., 60°/[11−1]), with each of them contributing nearly about 5% each (Fig. 3). It can also be observed that the population of twin-related intervariant boundary represented as V1-V2 (i.e., 60°/[11−1]) showed nearly a similar trend for all the three interfaces present in the microstructure, contributing about 5% of the total population.
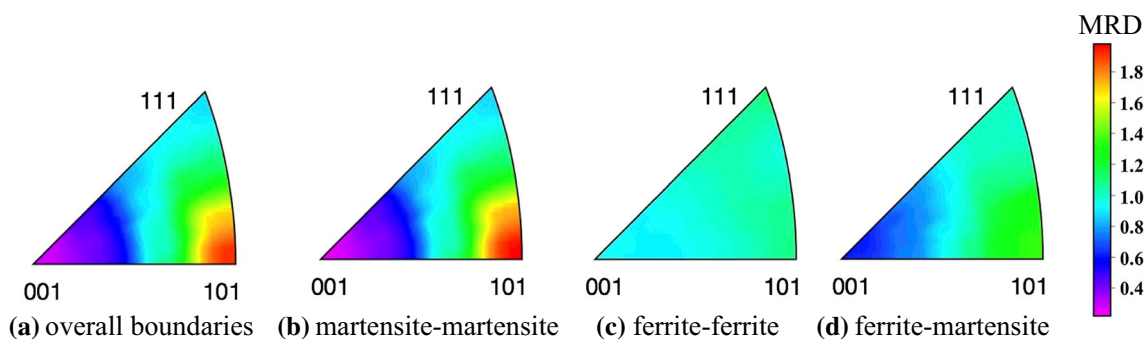
Grain boundary character distribution

The five-parameter grain boundary characterization approach was implemented to define the distribution of intervariant boundary planes character for different types of boundaries in the dual-phase microstructure. In the current study, the relative area of grain boundary planes, independent of misorientation, is displayed in stereographic projection in the crystal reference frame, where [001], [100] crystal axes were located perpendicular to the plane of the paper and horizontal to the right of the paper plane, respectively. The distribution of grain boundary planes for all misorientations exhibited an anisotropy for all types of interfaces (Fig. 4). The distributions for the overall microstructure, M–M and M-F interfaces are similar, having a peak at the position of (101) with a maxima of 1.92, 2 and 1.35 multiples of a random distribution (MRD), respectively. In other words, the population of (101) plane was 92%, 100% and 35% greater than expected in a random distribution, correspondingly (Fig. 4a, b, d). The minimum distribution was centred at (001) orientation for these
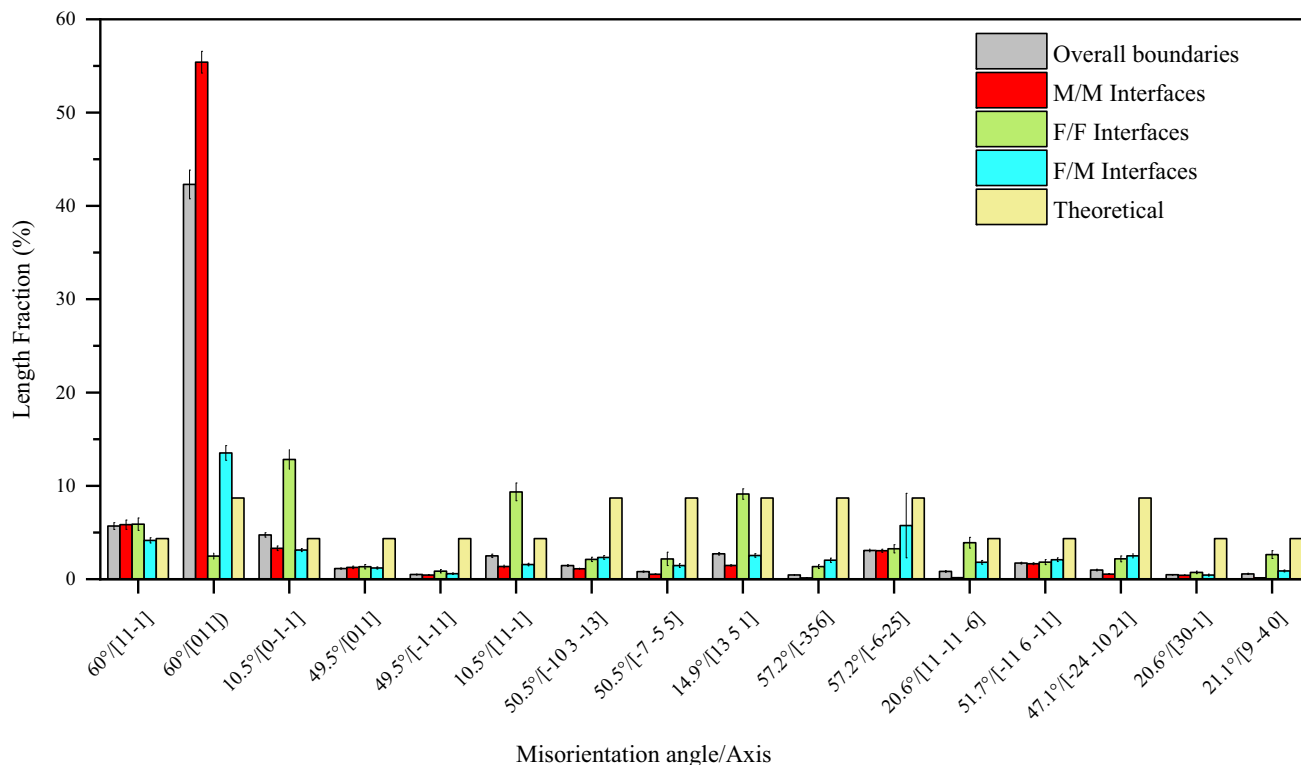
Figure 3 Fraction of total population of interfaces that corresponds to the KS OR detailing the intervariant interfaces between V1 and V*i* (*i* = 2–24) for different interface categories in the dual phase steel. M–M, F–F and F–M represent martensite–

martensite, ferrite–ferrite and ferrite–martensite interfaces, respectively. A 5° angular aperture was used to compute the length fraction of each intervariant boundary type.

(a) overall boundaries **(b)** martensite-martensite **(c)** ferrite-ferrite **(d)** ferrite-martensite

Figure 4 The distribution of grain boundary planes character for different interfaces, when the misorientation was ignored, in the dual phase steel. MRD represents multiples of a random distribution.

interfaces. Interestingly, the distribution was different for ferrite/ferrite interfaces, revealing weak anisotropy, having a maximum at the orientation of (111) with 1.13 MRD. The distribution was about 1.08 MRD at (101) and the minimum was located at the (001) orientation with 0.9 MRD (Fig. 4c).

Due to the relatively low carbon content of the steel (0.08% C), it was assumed that both the ferritic and martensitic transformations taking place during the

current heat treatment process follow the Kurdjumov–Sachs orientation relationship [10, 19]. Therefore, the distribution of intervariant grain boundary planes was plotted for the lattice misorientations, which correspond to the K-S orientation relationship (as listed in Table 1). For the overall microstructure, M–M and F–M interfaces, the distributions for these misorientations around the [011] axis were similar (Fig. 5). At 10.5°, the distribution revealed a single peak at the position of
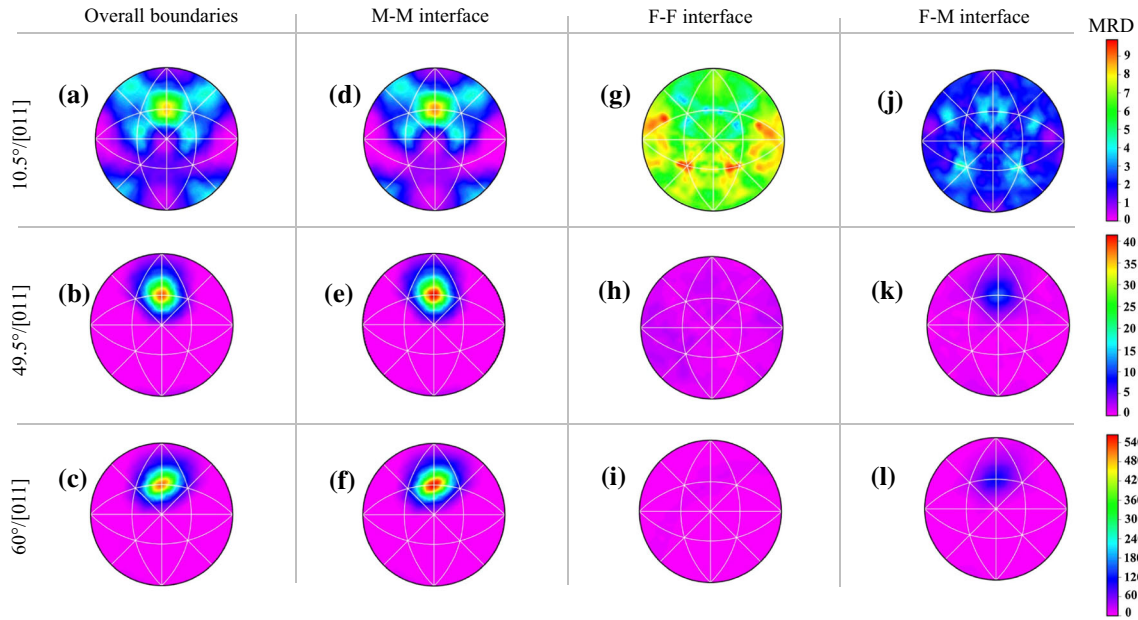
Figure 5 Distributions of plane normal for boundaries in dual phase steel having different misorientations around [110] axis. M–M, F–F and F–M represent martensite–martensite, ferrite–ferrite and ferrite–martensite interfaces, respectively.

{110}//{110} twist boundary having 8.4 and 8.9 MRD for overall and M–M interfaces, respectively (Figs. 5a,d). However, multiple peaks appeared for F–M interface with 4.9 MRD (Fig. 5j). The peak at the orientation of (110) with twist character progressively intensified with an increase in the misorientation angle to 49.5° and 60° for these three types of interfaces, revealing an intensity of about 490, 550 and 105 MRD for the overall, M–M and F–M interfaces, respectively (Figs. 5b,e,k).

The F–F interface distributions for the [011] misorientations were significantly different. At the misorientation angle of 10.53°, multiple peaks were observed, primarily centring at (1−11), (111), (−1−21) and (−121) with ∼ 10 MRD (Fig. 5g). With an increase in the misorientation angle to 49.5°, the peaks largely appeared at the same positions, though the intensity reduced to 2.7 MRD (Fig. 5h). At the misorientation angle of 60°, the distribution significantly altered revealing two peaks at (−1−1 2) and (−2 11) positions with 13.5 MRD (Fig. 5i).

For boundaries with a misorientation axis of <111>, the grain boundary plane distributions did not show a similar trend for all misorientation angles for a given interface type (Fig. 6). However, the distributions were nearly identical for overall microstructure and M–M interfaces for a given lattice misorientation. At a misorientation of 10.53°, the distribution revealed three peaks at the positions

close to (−1 −1 0), (0 −1 1) and (−1 0 1) having ∼ 5.3 MRD for overall and M–M interfaces (Fig. 6a, d). However, the distributions of F–M and F–F interfaces had multiple peaks at distinct positions having relatively higher intensities (Fig. 6g, j). The distribution significantly altered with an increase in the misorientation angle to 49.5°, revealing multiple peaks centred at the {110}//{110} symmetric tilt orientations for the overall and M–M interfaces (Fig. 6b, e), and {112}//{112} symmetric tilt orientations for F–F interfaces (Fig. 6h). Interestingly, the F–M interfaces revealed multiple peaks spread along the zone axis of tilt boundaries (Fig. 6k), resembling a superposition of the M–M and F–F distributions. At a misorientation of 60°, these distributions were similar to those at 49.5°, but with larger maxima. (Figs. 6c, f, i, l). The distribution of intervariant planes about the higher misorientation indices is also presented in Fig. 7. The distributions of these boundaries exhibited a single peak or multiple peaks about or close to {110} positions for all type of interfaces.

Discussion

The current study comprehensively characterizes different types of interfaces, namely martensite–martensite, ferrite–ferrite and ferrite–martensite in
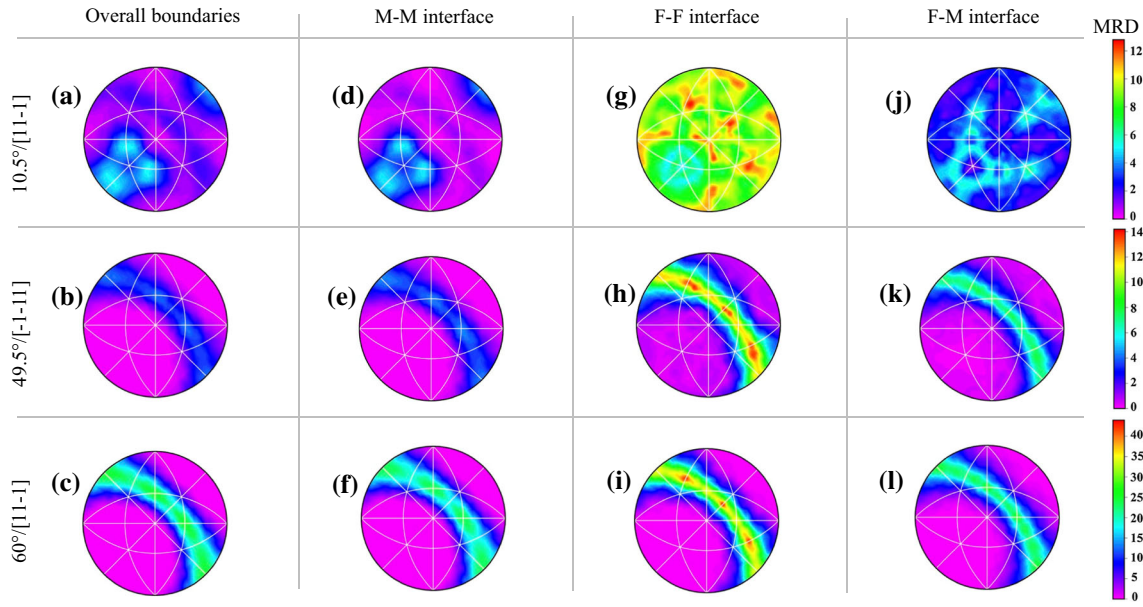
Figure 6 Distributions of plane normal for boundaries in dual phase steel having different misorientations around [111] axis. M–M, F–F and F–M represent martensite–martensite, ferrite–ferrite and ferrite–martensite interfaces, respectively.
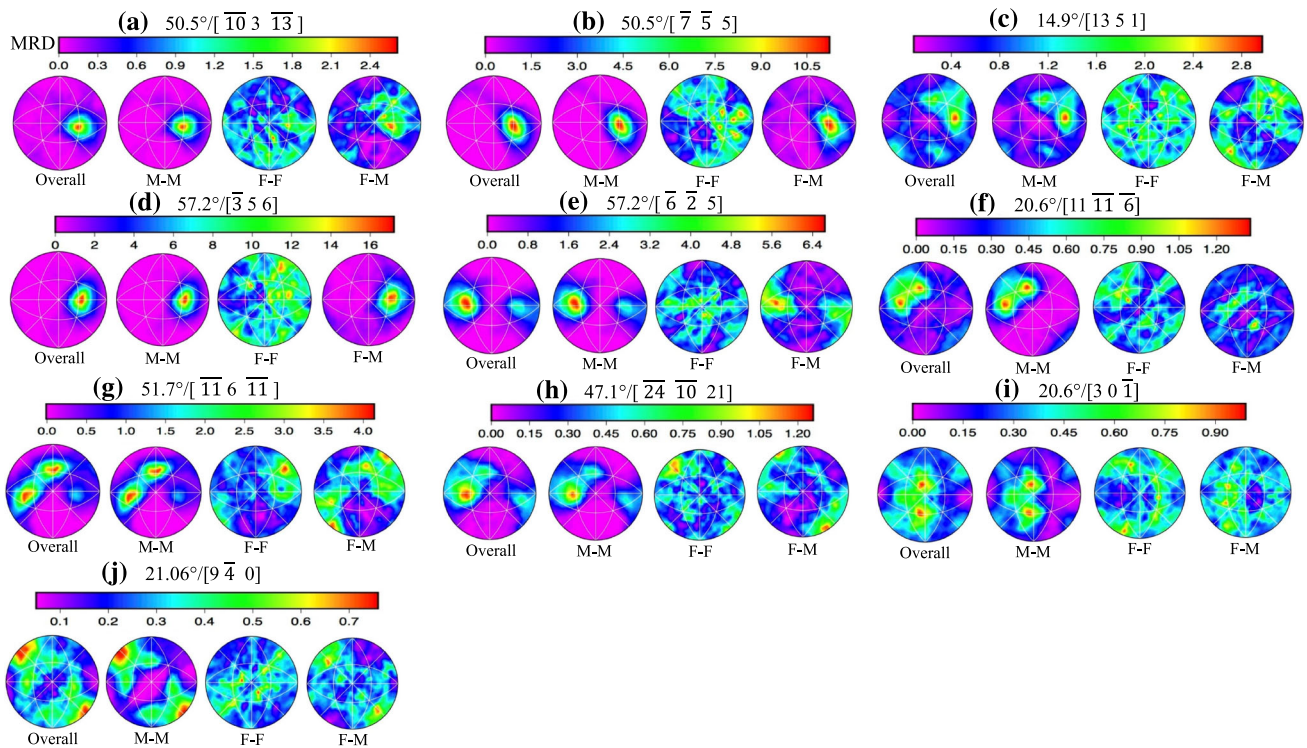
Figure 7 The distribution of boundary plane normals for boundaries with different misorientation angles and axes. M–M, F–F and F–M represent martensite–martensite, ferrite–ferrite and ferrite–martensite interfaces, respectively. MRD represents multiples of a random distribution.

steel with a dual-phase microstructure. Because these interfaces play a critical role in defining the deformation behaviour (strain partitioning, void nucleation, fracture etc.) in dual-phase steel, their distribution and detailed characterization can be used to establish structure–property correlations.

Misorientation angle distribution

Three types of interfaces present in the dual-phase microstructure (M–M, F–F and F–M) display distinct characteristics. However, the overall misorientation angle distribution is similar to the distribution of M–M interfaces. This is because the M–M interfaces constitute about 90% of the total grain boundary population measured in the current study. In other words, the M–M interfaces greatly outnumber the other two types and therefore dictate the grain boundary population distribution.

The most significant difference between the M–M and F–F distributions, is that the M–M distribution has no boundaries in the range of 22°–45° and a significant maximum at ∼ 60°, while the F–F distribution has interfaces spread across all misorientation angles up to 62.8°, with two broad maxima centred at about ∼ 13° and ∼ 60°. The distribution related to the F–M interfaces has a mixed character inherited from both M–M and F–F interfaces. These differences are the result of the phase transformation sequence taking place during cooling from the austenite regime, which results in the development of dual-phase microstructure in the present steel.

Upon cooling of austenite, the phase transformation initiates with the ferrite nucleation at the prior austenite grain boundaries as a result of a diffusional transformation. During isothermal holding at 625 °C, the prior austenite grain boundaries are largely consumed through the growth of ferrite grains, leaving behind the remanent austenite enveloped within the prior austenite grains. On subsequent quenching, the remanent austenite transforms into martensite. The transformation of austenite to the daughter phase (ferrite/martensite) in low carbon steel has been previously reported to largely follow the K–S orientation relationship [10], in which the parent phase can transform into 24 possible variants. Theoretically, the impingement of 24 variants from a single parent austenite grain results in 16 distinct lattice misorientations due to symmetry, which spread across 10 misorientation angles (10.53°, 14.88°, 20.61°, 21.06°, 47.11°, 49.47°, 50.51°, 51.73°, 57.21° and 60°), as listed in Table 1.

The misorientation angle distribution for M–M interfaces closely matches the misorientation angles expected from the intervariant boundaries predicted by the K-S orientation relationship (10°–21° and 47°–60°). In other words, the isolation of remanent austenite within ferrite grains significantly restricts the impingement of martensite islands formed from two distinct neighbouring prior austenite grains. As a result, the misorientation angles outside the ones related to the K-S OR do not appear in the distribution. On the contrary, the formation of ferrite grains on the prior austenite grain boundaries increases the chance of their impingement with the ones formed from neighbouring prior austenite grain, which most likely does not match the lattice misorientation expected from the K-S OR. Therefore, the subsequent misorientations may vary from 0 to 62.8°, which can explain the appearance of misorientations in the range of 22°–45° in the F–F misorientation angle distribution. A similar observation was reported for a fully ferritic microstructure elsewhere [21]. The same argument is valid for the F–M interfaces, where ferrite grains formed on the prior austenite grain boundaries may intersect with the martensite transformed in the neighbouring austenite, which does not follow the K-S OR with the grain boundary ferrite. However, the probability of this type of intersection is relatively less than that of a ferrite/ferrite intersection, resulting in a relatively lower population for misorientations in the range of 22°–45°.

Interface type on the intervariant boundaries population

It appears that the type of interface significantly influences the population of intervariant boundaries, which differ from the one expected from the theoretical calculation where each variant has equal chance to form within a parent austenite grain upon the phase transformation (Fig. 3). Generally, the grain boundary population is governed by different parameters, namely chemical composition, prior austenite grain size, thermo-mechanical processing parameters (i.e., strain, transformation temperature) and phase transformation mechanism. These parameters, indeed, influence the variant arrangement upon the phase transformation. This so-called variant selection process occurs to accommodate the strain associated with the phase transformation.

The current steel composition is prone to interphase precipitation during the ferrite transformation [17]. As a result, the carbon is mostly consumed by the formation of interphase precipitates within the ferrite, rather than moving to the adjacent austenite during the ferrite transformation. Therefore, the

chemical composition effect is ruled out here, as the carbon content of remaining austenite after the partial transformation to ferrite (i.e., martensite upon quenching) is expected to be close to the ferrite. The prior austenite grain is 270 ± 40 μm prior to the ferrite transformation. However, it is reduced for the subsequent martensitic transformation due to the partial ferrite transformation, which consumes a part of the prior austenite grain. The reduction in the prior austenite grain size is expected to limit the number of variants, which can form during the martensitic transformation. However, further work, beyond the scope of this study, would be required to confirm or refute this expectation.

The most striking difference in ferrite and martensite transformations is the temperature in which the transformation takes place and their phase transformation mechanism (i.e., diffusion vs shear). The nucleation of specific variants is governed by the rule of minimization of grain boundary energy and the strain energy accompanying the phase transformation. The ferrite transformation isothermally takes place at a temperature of 625 °C, though the martensite starts at a much lower temperature as the Ms temperature of the current alloy is calculated to be about 450 °C. The reduction in the phase transformation temperature enhances both the phase transformation driving force and the austenite strength. The latter increases the self-accommodation between variants, restricting their growth, resulting the microstructure refinement. This is evident here, as the martensitic microstructure is much finer than ferrite microstructure. The former leads to more frequent variant nucleation, suggesting that in any given austenite grain, more variants are nucleated during the martensitic transformation than during the ferrite transformation. Therefore, the impingement of martensitic variants formed within a prior austenite grain should promote the intervariant boundaries close to the theoretically calculated values in terms of the population if the variants are distributed randomly within a prior austenite grain. However, the population of intervariant boundaries formed in martensite significantly differs from the theoretically calculated one (Fig. 3), suggesting that a specific variant arrangement (i.e., variant selection) is promoted during the martensitic transformation.

In the case of the martensite–martensite interface, the population of intervariant boundaries is dominated by the variants originating from the same crystallographic family ($\{111\}_\gamma$ ||$\{110\}_\alpha$). These include 10.5°/[011], 60°/[111] and 60°/[011], constituting more than 60% of the total population. This suggests that the formation of variants largely occurs in a specific combination (e.g., V1-V3) to minimize or accommodate the transformation strain associated with the shear transformation. For instance, the intervariant boundaries formed as a result of two subsequent variants from the same family (e.g., V1-V2) is known to exhibit the twin relationship and cancel the transformation strain, promoting the progress of the martensitic transformation [13]. A similar trend was also observed for the fully martensitic microstructure in a 0.04C-1.52Mn, 0.2Si, 0.22Mo, 0.08Ti (in wt%), though the fraction of the intervariant boundaries differed from the current study [10].

Despite the fact that fewer ferrite variants are formed within each austenite grain due to the relatively high transformation temperature compared with martensite, the population of different intervariant boundaries in ferrite suggests that there is no specific variant arrangement taking place during ferrite transformation. This is not surprising as the strain/stress associated with ferrite transformation (diffusion) is much lower than martensite transformation (shear). In addition, the high-temperature transformation enhances the recovery of dislocations, which may form upon transformation. This leads to a distribution closer to the theoretically calculated one in ferrite (Fig. 3). This is consistent with the population of intervariant boundaries reported for the fully ferritic microstructure elsewhere [10]. The intervariant boundary population for the F–M interfaces appeared to be influenced by the distribution of intervariants for both the F–F and M–M interfaces.

Grain boundary plane distribution

The present results demonstrate the significant difference in the distribution of grain boundary planes for three different types of interfaces present in the dual-phase microstructure. This highlights the role of the phase transformation path on the interface characteristics, as the phase transformation mechanism changes from the diffusional for ferrite to displacive/shear for martensite during the development of the dual-phase microstructure.

It is well established that the relative areas of grain boundary planes are inversely related to their energies for polycrystalline materials evolving through

normal grain growth [11, 12]. This is consistent with the current result for ferrite/ferrite interfaces [11]. For instance, the distribution of grain boundary planes for 60°/[111] displays the maxima on {112} symmetric tilt boundary having the least energy for materials with body centred cubic (bcc) structure (i.e., ferrite–ferrite interface, Fig. 6i) [11, 19]. Unlike ferrite, the martensite grain boundary plane distribution for 60°/[111] exhibits maxima positioned at {110} symmetric tilt boundaries (Fig. 6f). This is primarily due to the fact that the martensitic transformation is displacive, closely following the crystallographic constraint associated with specific orientation relationship (here, the K-S OR). Therefore, the close-packed planes of the parent austenite match the close-packed plane of the martensite (i.e. $\{111\}_\gamma || \{110\}_{\alpha'}$) during transformation. This results in the likelihood of two crystallographic martensite variants terminating on {110} planes while intersecting during the transformation, which does not necessarily have the lowest energy configuration.

The ferrite–martensite interfaces, however, appears to inherit the characteristics features of both ferrite–ferrite and martensite–martensite interfaces. For example, the distribution of grain boundary planes for 60°/[111] is spread along the zone axis of tilt boundaries with the maxima positioned at {110} and {112} positions (Fig. 6l).

Conclusions

The relative areas of interfaces in the grain boundary network of a dual-phase steel comprised of equal proportions of ferrite and martensite were measured using the five-parameter approach. The present findings are summarized below:

1. The martensite–martensite interfaces displayed a bimodal misorientation angle distribution, having a dominate peak at ∼ 60°, which closely corresponded with the misorientation angle ranges expected from the K-S OR. The ferrite–ferrite misorientation angle distribution was spread across the entire misorientation range, having two broad peaks centred at ∼ 13° and ∼ 60°. The ferrite–martensite interfaces exhibited a mixed character inherited from both martensite and ferrite interface misorientation angle distributions.

2. There was a relatively strong anisotropy in the grain boundary plane orientations, ignoring misorientation, with a significant tendency to terminate on {110} planes for the martensite–martensite and ferrite–martensite interfaces.

3. The phase transformation mechanism significantly altered the grain boundary plane distribution for a given lattice misorientation. For the ferrite–ferrite interfaces, the 60°/[111] boundary, for example, displayed symmetrical tilt {112} boundary planes, which are known to be the low energy configuration. However, for the martensite–martensite interfaces, symmetrical tilt {110} boundaries result from the crystallographic constraint of the displacive phase transformation. The 60°/[111] misorientation showed multiple peaks along the zone of tilt boundaries for the ferrite–martensite interfaces, inherited from both diffusional ferrite and displacive martensite phase transformations.

4. In general, three different interfaces (martensite–martensite, ferrite–ferrite and ferrite–martensite) present in the dual-phase steel revealed distinct characteristics (i.e., population and plane orientation), which were dictated by the prominent phase transformation mechanism taking place during their formation.

Declarations

Conflict of interest The authors declare that they have no conflict of interest.

References

[1] Azuma M, Goutianos S, Hansen N, Winther G, Huang X (2012) Effect of hardness of martensite and ferrite on void formation in dual phase steel. Mater Sci Technol 28(9–10):1092–1100

[2] Calcagnotto M, Adachi Y, Ponge D, Raabe D (2011) Deformation and fracture mechanisms in fine- and ultrafine-grained ferrite/martensite dual-phase steels and the effect of aging. Acta Mater 59(2):658–670

[3] Sirinakorn T, Wongwises S, Uthaisangsuk V (2014) A study of local deformation and damage of dual phase steel. Mater Des 64:729–742

[4] Kadkhodapour J, Butz A, ZiaeiRad S (2011) Mechanisms of void formation during tensile testing in a commercial, dual-phase steel. Acta Mater 59(7):2575–2588

[5] Avramovic-Cingara G, Ososkov Y, Jain MK, Wilkinson DS (2009) Effect of martensite distribution on damage behaviour in DP600 dual phase steels. Mater Sci Eng, A 516(1):7–16

[6] Steinbrunner DL, Matlock DK, Krauss G (1988) Void formation during tensile testing of dual phase steels. Metall Trans A 19(3):579–589

[7] Park K, Nishiyama M, Nakada N, Tsuchiyama T, Takaki S (2014) Effect of the martensite distribution on the strain hardening and ductile fracture behaviors in dual-phase steel. Mater Sci Eng A 604:135–141

[8] Landron C, Bouaziz O, Maire E, Adrien J (2010) Characterization and modeling of void nucleation by interface decohesion in dual phase steels. Scripta Mater 63(10):973–976

[9] Kim C-S, Rollett AD, Rohrer GS (2006) Grain boundary planes: New dimensions in the grain boundary character distribution. Scripta Mater 54(6):1005–1009

[10] Beladi H, Rohrer GS, Rollett AD, Tari V, Hodgson PD (2014) The distribution of intervariant crystallographic planes in a lath martensite using five macroscopic parameters. Acta Mater 63:86–98

[11] Beladi H, Rohrer GS (2013) The relative grain boundary area and energy distributions in a ferritic steel determined from three-dimensional electron backscatter diffraction maps. Acta Mater 61(4):1404–1412

[12] Beladi H, Nuhfer NT, Rohrer GS (2014) The five-parameter grain boundary character and energy distributions of a fully austenitic high-manganese steel using three dimensional data. Acta Mater 70:281–289

[13] Kelly PM, Jostsons A, Blake RG (1990) The orientation relationship between lath martensite and austenite in low carbon, low alloy steels. Acta Metall Mater 38(6):1075–1081

[14] Beladi H, Tari V, Timokhina IB, Cizek P, Rohrer GS, Rollett AD, Hodgson PD (2017) On the crystallographic characteristics of nanobainitic steel. Acta Mater 127:426–437

[15] Zhong X, Rowenhorst DJ, Beladi H, Rohrer GS (2017) The five-parameter grain boundary curvature distribution in an austenitic and ferritic steel. Acta Mater 123:136–145

[16] Haghdadi N, Cizek P, Hodgson PD, Beladi H (2019) Microstructure dependence of impact toughness in duplex stainless steels. Mater Sci Eng, A 745:369–378

[17] Bikmukhametov I, Beladi H, Wang J, Hodgson PD, Timokhina I (2019) The effect of strain on interphase precipitation characteristics in a Ti-Mo steel. Acta Mater 170:75–86

[18] Saylor DM, El-Dasher BS, Adams BL, Rohrer GS (2004) Measuring the five-parameter grain-boundary distribution from observations of planar sections. Metall and Mater Trans A 35(7):1981–1989

[19] Miyamoto G, Iwata N, Takayama N, Furuhara T (2012) Quantitative analysis of variant selection in ausformed lath martensite. Acta Mater 60(3):1139–1148

[20] Flower HM, Lindley TC (2000) Electron backscattering diffraction study of acicular ferrite, bainite, and martensite steel microstructures. Mater Sci Technol 16(1):26–40

[21] Beladi H, Rohrer GS (2016) The Role of Thermomechanical Routes on the Distribution of Grain Boundary and Interface Plane Orientations in Transformed Microstructures. Metall and Mater Trans A 48(6):2781–2790